Anti-Aesthetics: Protecting Facial Privacy against Customized Text-to-Image Synthesis

Songping Wang, Yueming Lyu†, Shiqi Liu, Ning Li, Tong Tong, Hao Sun, Caifeng Shan†, Senior Member, IEEE

***Abstract*—The rise of customized diffusion models has spurred a boom in personalized visual content creation, but also poses risks of malicious misuse, severely threatening personal privacy and copyright protection. Some studies show that the aesthetic properties of images are highly positively correlated with human perception of image quality. Inspired by this, we approach the problem from a novel and intriguing aesthetic perspective to degrade the generation quality of maliciously customized models, thereby achieving better protection of facial identity. Specifically, we propose a Hierarchical Anti-Aesthetic (HAA) framework to fully explore aesthetic cues, which consists of two key branches: 1) Global Anti-Aesthetics: By establishing a global anti-aesthetic reward mechanism and a global anti-aesthetic loss, it can degrade the overall aesthetics of the generated content; 2) Local Anti-Aesthetics: A local anti-aesthetic reward mechanism and a local anti-aesthetic loss are designed to guide adversarial perturbations to disrupt local facial identity. By seamlessly integrating both branches, our HAA effectively achieves the goal of anti-aesthetics from a global to a local level during customized generation. Extensive experiments show that HAA outperforms existing SOTA methods largely in identity removal, providing a powerful tool for protecting facial privacy and copyright.**

***Index Terms*—Facialprivacyprotection, diffusionmodel, text-to-imagesynthesis, adversarialattacks**

I. Introduction

DIFFUSION models (DMs) achieve significant breakthroughs in the field of text-to-image (T2I) generation, markedly enhancing the quality and realism of image generation by executing diffusion processes in latent spaces [1], [2], [3], [4], [5], [6], [7]. These models diversify and enhanced visual effects in image generation while ensuring a high degree of consistency between the generated images and textual descriptions. To meet personalized needs and improve fine-tuning efficiency, researchers develop various DMs fine-tuning methods, such as Textual Inversion [8], DreamBooth [9], Custom Diffusion [10], and SVDiff [11]. These fine-tuning methods offer higher customization capabilities, allowing users to generate high-quality images of specific themes with few reference images.

Despite the immense potential of these technologies, they also harbor significant safety risks that cannot be ignored. Malicious users may exploit these models to generate forged images or deepfake content, infringing on personal privacy and intellectual property rights, and even creating fake news to mislead the public [12], [13], [14].

To address these threats, anti-customization methods are primarily based on adversarial attacks, such as Mist [15], ASPL [16] and CAAT [17]. These methods introduce adversarial noises to interfere with the customized fine-tuning process, preventing the malicious misuse of user images by customized diffusion models. However, as illustrated in Figure 1, existing methods exhibit limitations in facial privacy protection and copyright preservation. These approaches primarily rely on a straightforward end-to-end paradigm that degrades overall image quality by maximizing the original training loss, yet they critically overlook the design of identity elimination for local facial regions. This oversight substantially undermines their effectiveness in removing recognizable facial features, potentially leading to privacy leakage and the misuse of user portraits.

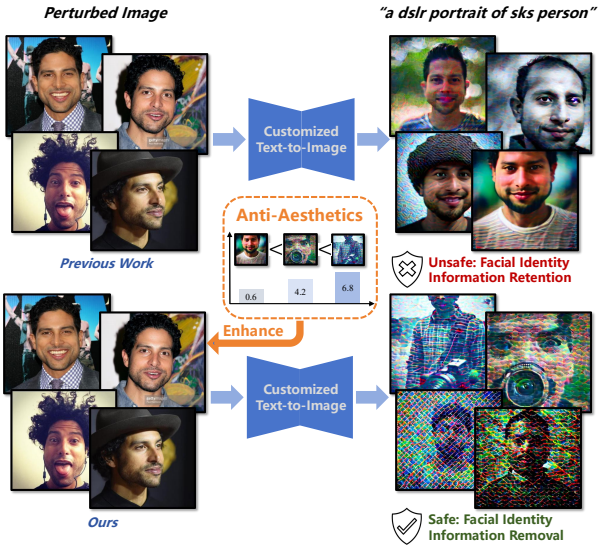

Fig. 1. Previous work for protecting images overlook aesthetic cues, which limits their ability to remove identity and inevitably leads to privacy leakage. In contrast, our method effectively enhances the ability to eliminate facial identity guided by proposed anti-aesthetic mechanisms. The prompt is "a dslr portrait of sks person".

To delve into this issue, we have the following key observations and reflections from a novel aesthetic perspective: 1) There is a close and inseparable connection between the aesthetic attributes of an image and human perception of image quality [18]. Specifically, the higher the conformity of an image to aesthetic standards, the higher its quality; conversely, the more an image deviates from aesthetic standards, the lower its quality. 2) Human aesthetic perception is not a single dimension, but hierarchical, encompassing both the perception of global harmony and the perception of local details. These two levels of aesthetic perception together form a comprehensive judgment of image aesthetics [19]. 3) The observational findings depicted in Figure 2 demonstrate that aligning with human

†Corresponding author

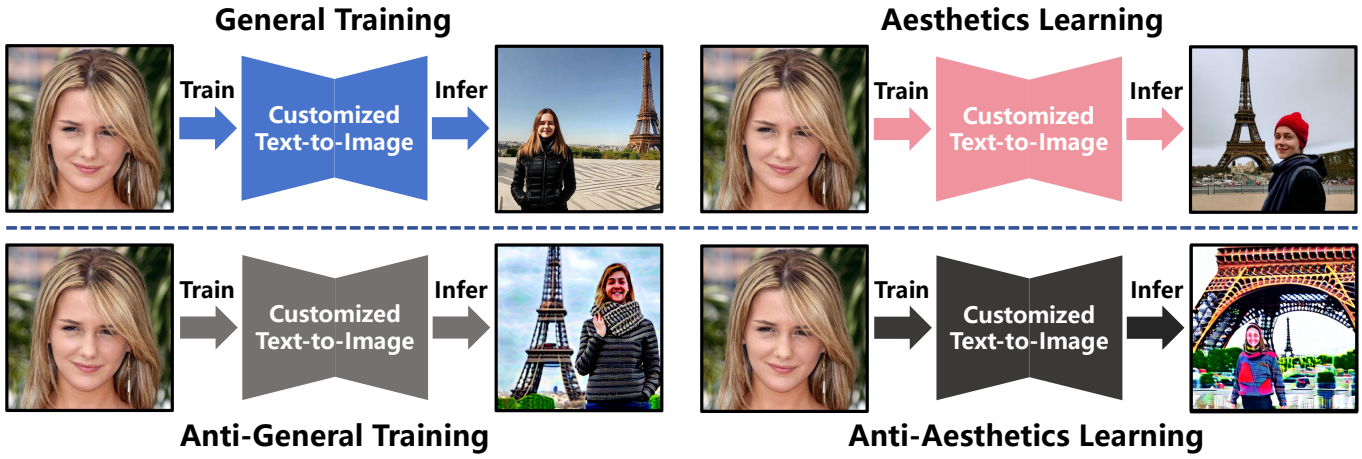

Fig. 2. Compared with general training, aesthetic learning enhances the quality and details of generated images by aligning with human aesthetic preferences. Similarly, Compared with anti-general training (previous protection methods), anti-aesthetic learning further reduces the quality of generated images and destroys facial details by misaligning with human aesthetics, thereby effectively protecting facial privacy. "a photo of a sks person in front of the Eiffel Tower" used as the prompt for inference.

aesthetic preferences can effectively improve the quality of generated images and facial details. [20], [21]. Thus, we can't help but wonder: ***If we adopt an anti-aesthetic alignment approach, could it possibly achieve the goal of reducing the quality of generated images and removing facial identity?***

Inspired by the above observations and reflections, we propose the Hierarchical Anti-Aesthetic (HAA) framework. This framework is designed to degrade image quality by hierarchically exploring aesthetic cues from global to local scales, thereby safeguarding users' facial privacy and copyright. Specifically, HAA includes the following two key branches: 1) Global Anti-Aesthetics, which weakens the overall aesthetics of images generated by malicious fine-tuners and reduces the overall quality of image generation by constructing a global anti-aesthetic reward mechanism and designing a global anti-aesthetic loss. 2) Local Anti-Aesthetics, which guides adversarial noises to force customized diffusion models to perform local anti-facial aesthetic alignment by carefully establishing a local anti-aesthetic reward mechanism and designing a local anti-aesthetic loss, thereby reducing their ability to reconstruct facial details. By seamlessly integrating the above branches, we form a joint hierarchical anti-aesthetic framework, which fully explores aesthetic clues from global to local to achieve the goal of anti-aesthetics. The implementation of anti-aesthetics greatly reduces the generation quality of customized DMs, thereby reducing facial identity leakage and enhancing the ability to protect personal privacy and copyright. Our main contributions are as follows:

- From a novel and intriguing aesthetic perspective, we propose a joint Hierarchical Anti-Aesthetic (HAA) framework that seamlessly integrates global and local anti-aesthetic branches. This integration effectively reduces aesthetic features across both global and local levels, thereby achieving the goal of anti-aesthetics.
- We introduce Global Anti-Aesthetics by carefully constructing a global anti-aesthetic reward mechanism and designing a global anti-aesthetic loss, thereby reducing the overall generation quality of customized generative models.
- We propose Local Anti-Aesthetics, construct a local anti-aesthetic reward mechanism, and design a local anti-aesthetic loss to guide malicious customized diffusion models to oppose alignment with human facial aesthetics.
- Extensive experiments across multiple datasets and generative models demonstrate that our approach outperforms existing state-of-the-art methods largely, proving the effectiveness and generalization capability of our method.

II. RELATED WORK

A. Customized Diffusion Models

Recent years have witnessed continued development of diffusion models [4], [5], [6], [7], [22], [23], showing great potential in guiding the generation process through text input. The exemplar models, including DALL-E 2 [3], Stable Diffusion [2] and Stable Diffusion XL [24], have received wide attention for their high sample quality. Using the latent diffusion method and incorporating CLIP-based [25] text encoders, these models utilize a two-stage process: encoding the input image or text into a latent representation and denoising within this compact latent space to effectively bridge the gap between textual descriptions and visual content, which significantly improves the generation quality while maintaining high fidelity and consistency in text-to-image (T2I) generation tasks.

Dreambooth [9] further addresses the challenge of customized generation, leading to significant improvements in generating personalized content from limited data while preserving the diversity and flexibility. However, Dreambooth faces challenges with more complex customizations, particularly when the personalization demands a diverse and extensive dataset. In contrast, Custom Diffusion [10] can first fine-tune each concept model individually, and then merge them into one through constrained optimization, which enhances the ability to generate diverse outputs while maintaining coherence across different concepts. SVDiff [11] optimizes all the singular values of the weight matrix, and leverages spectral shifts to

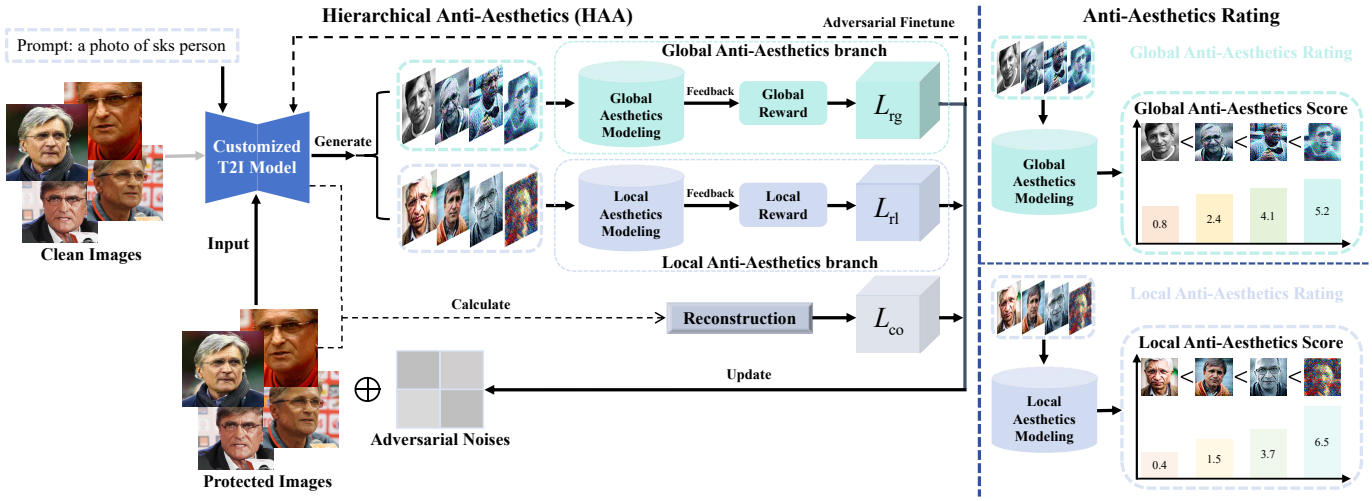

Fig. 3. The framework of our proposed method. It is an iterative training process where the adversarial noise and the parameters of the surrogate customized generative model are updated simultaneously. The final adversarial noise generated is added to the user's image, making it resistant to malicious use by the customized generative model.

introduce a small number of trainable parameters into diffusion models, enabling them to effectively capture variations in specific themes. Textual Inversion [8] teaches a text model a new word using example images, training its embedding to align with the corresponding visual representation by adding a new token to the vocabulary and training with representative images.

B. Privacy Protection with Image Cloaking

Recent breakthroughs in generative models, represented by diffusion models, have achieved paradigm-shifting advancements. Building on this foundation, the development of customization technologies has greatly facilitated personal visual creation. However, the misuse of personalized custom generation has raised significant concerns about copyright protection, political stability, and the potential security of personal privacy data. To address these issues, image cloaking methods have been developed, which involve adding specific perturbations to the original images to prevent misuse by customized generative models.

AdvDM [26] performs Monte Carlo sampling on latent variables in the diffusion model's hidden space and generates perturbations specifically targeting and misleading the model's feature extraction process during the sampling time steps, ultimately leading the model to produce erroneous outputs or reducing its overall performance. ASPL [16] employs an Alternating Surrogate and Perturbation Learning (ASPL) strategy to enhance counterattacks against DreamBooth method. It adopts a strategy of alternating between clean samples and adversarial samples to train the surrogate model, thereby promoting the generation of more destructive perturbations and refining the perturbation strategy to optimize its effectiveness. Mist [15] is specifically designed for copyright protection of artwork and can effectively defend against malicious use of methods such as Lora and SDEdit. CAAT [17] effectively disrupts the text-to-image mapping by introducing subtle perturbations in the cross-attention layers of customized diffusion models, thereby protecting users' portrait rights from infringement. SimAC [27] explores the limitations of the internal properties of diffusion models, investigates the relationship between time step selection and frequency domain perception as well as the roles of hierarchical features in the denoising process, and proposes an adaptive greedy time step search and a feature-based optimization framework, which enhances the anti-interference effect.

However, the aforementioned methods primarily rely on a straightforward end-to-end paradigm to maximize the original training loss, neglecting the aesthetic clues hidden in the images, which limits their ability to remove facial identity information. Our method fills this gap through a Hierarchical Anti-Aesthetic framework, fully exploring aesthetic clues from global to local to effectively protect facial privacy.

III. THE PROPOSED METHOD

Figure 3 illustrates our Hierarchical Anti-Aesthetic (HAA) framework, which degrades image quality by leveraging global harmony and local detail perception in human aesthetics. Through carefully designed global and local anti-aesthetic reward mechanisms and their corresponding loss functions, HAA effectively reduces facial identity leakage in customized diffusion models by enforcing anti-alignment with human aesthetic preferences. We introduce the principles of DreamBooth and adversarial attacks in Section 3.1, followed by the global anti-aesthetics in Section 3.2 and local anti-aesthetics in Section 3.3. Finally, we present our HAA framework in Section 3.4.

A. Preliminaries

DreamBooth is a classic fine-tuning technique for text-to-Image diffusion Models that enables personalized generation. Specifically, given a small number (3-5) of subject images, it fine-tunes a pre-trained DM to generate new images of that subject in various contexts. DreamBooth binds the target

subject with a rare token identifier (e.g., sks), and the input prompt follows the format of 'a sks [class noun]', where [class noun] represents the category (e.g., person). DreamBooth combines two objective loss functions, including a personalization reconstruction loss and a prior preservation loss. The personalization reconstruction loss aims to make the generated images highly consistent with the given reference subject, while the prior preservation loss prevents overfitting and text drift issues in the case of few-shot instances. By combining these two losses, DreamBooth achieves high-quality, customized image generation. The formulation is as follows:

$$\begin{aligned}\mathcal{L}_{co}(v_0,\theta) = \mathbb{E}_{v_0,c,t,t'}\|\epsilon - \epsilon_\theta(v_{t+1},c,t)\|_2^2 \\ +\gamma\cdot\|\epsilon' - \epsilon_\theta(v'_{t'+1},c_{pr},t')\|_2^2,\end{aligned} \tag{1}$$

where ϵ_θ denotes the function of the diffusion model, parameterized by θ. v_0 signifies the initial input image, while c and c_{pr} represent the prompt and the prior prompt, respectively. t and t' correspond to distinct time steps within the diffusion process. ϵ and ϵ' are both sampled from $\mathcal{N}(0,I)$. v refers to noisy latent and v' denotes noisy latent of the class example. γ is a tuning coefficient, while $\|_2^2\cdot\|_2^2$ represents the square of the second norm.

Adversarial attacks are widely applied in various fields, revealing the vulnerability of deep neural networks, which serve as the cornerstone of modern artifacial intelligence. Adversarial attacks initially refer to the process of adding subtle and imperceptible disturbances δ to a given input x, causing model f to produce incorrect outputs with high confidence that differ from their true labels y. The formula is represented as follows:

$$x_{adv} = x + Proj(\alpha * L(f(x+\delta),y)), \tag{2}$$

where L is the loss function. $Proj(\cdot)$ ensures that the adversarial noise remains within the reasonable range. α represents the learining rate, while x_{adv} denotes the adversarial examples.

B. Global Anti-Aesthetics (GAA)

We start from a novel perspective—the relationship between aesthetics and quality—and introduce a novel Global Anti-aesthetic Algorithm (GAA), which focuses on mining global aesthetic clues to degrade the overall quality of images. Specifically, we construct a global anti-aesthetic reward mechanism and design a global anti-aesthetic loss function in conjunction with a reconstruction loss to train adversarial noise.

Global anti-aesthetic reward mechanism. Given a sample x, we perform diffusion steps on it using a pre-trained surrogate DM. Then, we employ a Monte Carlo sampling strategy to sample adversarial latents for global anti-aesthetic alignment and map them back to the pixel space using a decoder. This process can be formalized as follows:

$$x'_t = G_{\theta_t}(N(E(x_t^{adv}),B(T)),C), \tag{3}$$

where x_t^{adv} denotes the adversarial sample at the t-th iteration, $B(\cdot)$ signifies the Monte Carlo sampling function, T stands for the set of diffusion time steps, C represents the input prompt, $E(\cdot)$ denotes the encoder, $N(\cdot)$ indicates the noise scheduler, and $G_\theta(\cdot)$ is the function that maps the latent space back to the image domain, parameterized by θ.

To implement the Global Anti-Aesthetic (GAA), we need to construct a global anti-aesthetic reward model to obtain global anti-aesthetic rewards. For this purpose, we utilize the publicly available human aesthetic preference dataset VisionRewardDB-Image [28] to train a Global Aesthetic Reward Model RM_g with BLIP as the backbone. Through RM_g, we can conduct a global aesthetic evaluation of the generated images to obtain global aesthetic scores. Subsequently, we ingeniously construct global anti-aesthetic rewards R_i^g using these global aesthetic scores. The formulas can be expressed as follows:

$$r_i^g = |RM_g(x_i^o,C_g) - RM_g(x'_{ti},C_g)| - RM_g(x'_{ti},C_g), \tag{4}$$

$$R_i^g = \frac{r_i^g - \frac{1}{n}\sum_{i=1}^n r_i^g}{\sqrt{\frac{1}{n}\sum_{i=1}^n (r_i^g - \frac{1}{n}\sum_{i=1}^n r_i^g)^2}}, \tag{5}$$

let x'_{ti} represent the i-th generated sample in the batch at the t-th iteration, where n denotes the batch size. x_i^o denotes the i-th original image. C_g represents the global prompt and $|\cdot|$ indicates the absolute value function. The larger the value of R_i^g, the higher the global anti-aesthetic score and the poorer the overall quality of the generated image.

Global anti-aesthetic loss. In our approach, we utilize the global anti-aesthetic reward R_i^g obtained from Eq.5 to calculate the global anti-aesthetic loss $\mathcal{L}_{rg}$. This loss is then employed to update the adversarial noise, which in turn guides the adversarial noise to undermine the overall generation quality of malicious fine-tuners. The specific formula for the calculation is as follows:

$$\mathcal{L}_{rg} = \frac{1}{n}\sum_{i=1}^n \exp(R_i^g), \tag{6}$$

$$\mathbf{g}_{t+1}^{adv} = \mu\cdot\mathbf{g}_t^{adv} + \frac{\nabla_{\mathbf{x}}(\mathcal{L}_{co}+\lambda\cdot\mathcal{L}_{rg})}{\|\nabla_{\mathbf{x}}(\mathcal{L}_{co}+\lambda\cdot\mathcal{L}_{rg})\|_1}, \tag{7}$$

$$x_{t+1}^{adv} = Proj(x_t^{adv} + \alpha * sign(\mathbf{g}_{t+1}^{adv})), \tag{8}$$

where $exp(\cdot)$ is the exponential function, $\mathcal{L}_{co}$ is the reconstruction loss, defined in Eq. 1, μ and λ are balancing coefficients, g_t^{adv} is the t-th adversarial gradient, and $sign(\cdot)$ is the sign function.

In addition, during the training process of GAA, we also optimize the surrogate diffusion model (SDM) simultaneously. Specifically, SDM is trained on the carefully constructed adversarial samples x_{adv}, thereby enhance the robustness of the models themselves. The training process of the above SDM can be represented in the following form:

$$\theta' = \arg\min_{\theta'} \mathcal{L}_{co}(x_{adv},\theta'), \tag{9}$$

where θ' is the parameter of SDM. Based on this, the obtained adversarial samples are further applied to the optimized SDM with enhanced robustness. Through this interactive mechanism, adversarial samples with more powerful attack effects can be generated, thereby improving the overall attack capability.

C. Local Anti-Aesthetics (LAA)

Human perception of aesthetics is multidimensional, encompassing not onlyglobal aesthetic perception but also local aesthetic perception. Inspired by this, we propose a novel Local Anti-Aesthetic Algorithm (LAA), where we construct a local anti-aesthetic reward mechanism and design a local anti-aesthetic loss. This approach forces maliciously fine-tuned DMs to perform anti-facial aesthetic alignment, thereby enhancing the ability to eliminate facial identity cues.

Local anti-aesthetic reward mechanism. Specifically, a lightweight face detection model F is used to identify the x'_t defined in Eq. 3, obtaining facial boxes Box_t and confidence scores S. Similar to the global aesthetic reward model, to mine local facial aesthetic clues, we use the same BLIP architecture to construct a low-cost local facial aesthetic reward model RM_l. Incorporating the obtained boxes and the generated images, we can extract the corresponding facial images and use the RM_l to provide local aesthetics feedback. Then we utilize the feedback to calculate the local anti-aesthetics rewards R_i^l for updating the adversarial noise. The worse the quality of the generated face, the higher the R_i^l. This process can be formalized as follows:

$$S_{ti}, Box_{ti} = F(x'_{ti}), \tag{10}$$

$$r_i^l = -RM_l(x'_{ti}, Box_{ti}), \tag{11}$$

$$R_i^l = \frac{r_i^l - \frac{1}{n}\sum_{i=1}^{n} r_i^l}{\sqrt{\frac{1}{n}\sum_{i=1}^{n}(r_i^l - \frac{1}{n}\sum_{i=1}^{n} r_i^l)^2}}. \tag{12}$$

Local anti-aesthetic loss. Based on R_i^l, we can further calculate the reward loss $\mathcal{L}_{rl}$ for the update of adversarial noises. This process can be formalized as follows:

$$\mathcal{L}_{rl} = \frac{1}{n}\sum_{i=1}^{n} \exp(R_i^l), \tag{13}$$

$$x_{adv} = Proj(\arg\max_{x_{adv}}(\mathcal{L}_{co} + \beta \cdot \mathcal{L}_{rl})), \tag{14}$$

where β is the balancing coefficient. Similarly, the parameters of the surrogate diffusion model are also updated during the iterative attack. By attacking more robust surrogate diffusion models, the intensity of the attack is enhanced, thereby achieving the local anti-aesthetic objective.

D. Hierarchical Anti-Aesthetics (HAA)

Building upon the individual strengths of Global Anti-Aesthetics (GAA) and Local Anti-Aesthetics (LAA), we propose a unified Hierarchical Anti-Aesthetic (HAA) framework that synergistically combines both global and local aesthetic degradation strategies. This integrated approach enables comprehensive disruption of image generation quality at multiple perceptual levels, thereby achieving anti-aesthetics from global to local. Combining $\mathcal{L}_{total}$, $\mathcal{L}_{rg}$ and $\mathcal{L}_{rl}$, we calculate the final total loss for joint optimization, which is expressed by the following formula:

$$\mathcal{L}_{total} = \mathcal{L}_{co} + \lambda \cdot \mathcal{L}_{rg} + \beta \cdot \mathcal{L}_{rl}. \tag{15}$$

$$x_{adv} = Proj(\arg\max_{x_{adv}}(\mathcal{L}_{total})). \tag{16}$$

In each iteration of the attack, the overall loss is maximized to optimize the adversarial samples, enabling the adversarial noise to effectively learn how to poison malicious fine-tuners and disrupt the global and local aesthetics of their generated images, thereby significantly degrading the overall quality of the images. While the adversarial samples are iteratively optimized, the parameters of the surrogate DM are fine-tuned in an adversarial training-like manner. Ultimately, through iterative attacks, the final adversarial samples can effectively remove facial identity information, thereby protecting facial privacy and copyright.

IV. EXPERIMENTS

A. Experimental Settings

Datasets. Following previous work [17], we conduct experiments using the Celeb-HQ [29] and VGGFace2 [30] datasets. Both of them are large classic facial datasets specifically for computer vision research. Due to the wide range of comparison metrics, we select 10 individuals from each dataset, covering different genders, ages, and ethnicities, with at least 15 images for each individual.

Models. Our experiments primarily utilize the popular open-source diffusion model SD-v2.1 [31]. Furthermore, to extensively validate the effectiveness of our approach, we also conduct experiments on SD-v1.4 [32] and SD-v1.5 [31].

Baselines and comparisons. We compare our method with various state of the art methods designed to prevent the misuse of user images by DMs, including ASPL [16], Mist [15], CAAT [17] and SimAC [27].

Metrics. Following previous work [17], we employ a facial detection model to detect the generated images, calculating the metric Facial Detection Success Rate (FDSR) [33], and for images where faces are detected, we calculate the Face Similarity [34] between the detected faces and clean images. Moreover, Image Reward [28] is used to assess the quality of the generated images, calculating its evaluation score metric IR. Finally, Fréchet Inception Distance (FID) [35] is used to assess the similarity between the generated images and clean images.

Implementation Details. We use the latest Stable Diffusion (v2.1) as the pre-trained model and fine-tune the text encoder and UNet models using the DreamBooth method for 500 training steps with a batch size of 1 and a learning rate of 5×10^{-7}. We set eps=0.06 for the noise budget and $\alpha = 0.002$ for the noise learning rate. More details are shown in supplementary materials.

B. Comparison with Baselines

To comprehensively evaluate the effectiveness of our method, we conduct quantitative comparative experiments on two datasets (CelebA-HQ and VGG-Face2) with four different prompt settings (three of which were unseen during training) against state-of-the-art methods in Table I and Table II. For each prompt, we randomly generate 16 images and calculated the average values of four metrics. For FDSR, Face Similarity, and Image Reward, lower values indicate better protection effects, while higher FID values indicate better protection

TABLE I
PERFORMANCE ON CELEBA-HQ DATASET.

CelebA-HQ				
Method	"a photo of sks person"			
	FDSR↓	Face Similarity↓	Image Reward↓	FID↑
Clean	1.000	0.498	0.599	112.3
Mist	0.969	0.375	0.191	281.2
CAAT	0.813	0.339	0.326	271.7
ASPL	0.750	0.332	0.006	359.5
SimAC	0.438	0.321	-0.188	388.9
HAA	**0.281**	**0.117**	**-0.894**	**471.1**
Method	"a dslr portrait of sks person"			
	FDSR↓	Face Similarity↓	Image Reward↓	FID↑
Clean	0.859	0.346	0.706	175.1
Mist	0.859	0.308	0.249	271.0
CAAT	0.766	0.260	0.236	251.8
ASPL	0.656	0.251	-0.183	384.0
SimAC	0.500	0.239	-0.202	369.0
HAA	**0.266**	**0.115**	**-0.861**	**461.4**
Method	"a close-up photo of sks person, high details"			
	FDSR↓	Face Similarity↓	Image Reward↓	FID↑
Clean	0.625	0.276	0.281	200.8
Mist	0.594	0.268	-0.128	268.4
CAAT	0.510	0.177	-0.419	305.9
ASPL	0.438	0.167	-0.882	433.3
SimAC	0.333	0.162	-0.779	401.7
HAA	**0.177**	**0.077**	**-1.334**	**476.0**
Method	"a photo of sks person looking at the mirror"			
	FDSR↓	Face Similarity↓	Image Reward↓	FID↑
Clean	0.672	0.276	0.022	232.9
Mist	0.695	0.257	-0.289	287.0
CAAT	0.602	0.171	-0.545	316.1
ASPL	0.523	0.157	-0.854	422.4
SimAC	0.562	0.156	-0.773	405.6
HAA	**0.289**	**0.085**	**-1.296**	**473.5**

TABLE II
PERFORMANCE ON VGG-FACE2 DATASET.

VGG-Face2				
Method	"a photo of sks person"			
	FDSR↓	Face Similarity↓	Image Reward↓	FID↑
Clean	0.875	0.421	0.625	199.1
Mist	0.906	0.227	0.248	355.6
CAAT	0.719	0.145	0.371	349.8
ASPL	0.750	0.193	0.373	388.6
SimAC	0.500	0.118	0.143	435.6
HAA	**0.125**	**0.031**	**-0.252**	**468.6**
Method	"a dslr portrait of sks person"			
	FDSR↓	Face Similarity↓	Image Reward↓	FID↑
Clean	0.813	0.379	0.717	227.6
Mist	0.813	0.240	0.409	357.2
CAAT	0.750	0.179	0.559	332.8
ASPL	0.703	0.173	0.351	387.9
SimAC	0.422	0.102	-0.018	429.3
HAA	**0.109**	**0.028**	**-0.608**	**462.4**
Method	"a close-up photo of sks person, high details"			
	FDSR↓	Face Similarity↓	Image Reward↓	FID↑
Clean	0.688	0.376	0.720	232.3
Mist	0.573	0.215	0.279	343.2
CAAT	0.521	0.155	0.353	341.1
ASPL	0.490	0.150	0.039	381.0
SimAC	0.292	0.078	-0.581	434.5
HAA	**0.083**	**0.019**	**-1.162**	**458.4**
Method	"a photo of sks person looking at the mirror"			
	FDSR↓	Face Similarity↓	Image Reward↓	FID↑
Clean	0.750	0.355	0.482	246.0
Mist	0.641	0.188	0.005	354.9
CAAT	0.633	0.139	0.145	334.0
ASPL	0.602	0.153	-0.055	380.6
SimAC	0.414	0.092	-0.616	429.0
HAA	**0.258**	**0.031**	**-1.119**	**446.0**

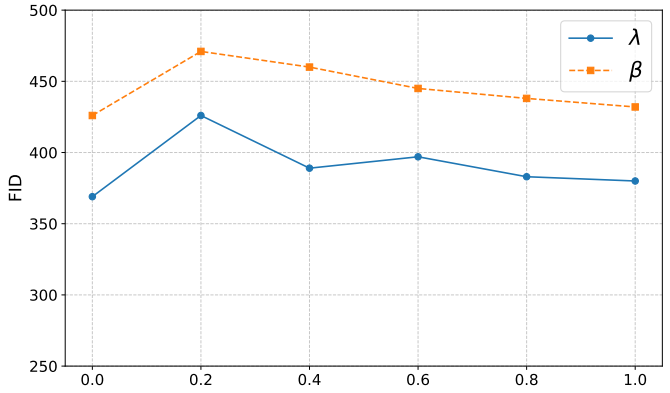

Fig. 4. FID value varies with different λ and β values defined in Eq. 15.

effects. On the CelebA-HQ dataset with the prompt "a photo of sks person", HAA achieved a 68.8% reduction in FDSR (from 96.9% to 28.1%), a 25.8% reduction in Face Similarity (from 37.5% to 11.7%), and a 468.1% reduction in Image Reward (from 0.191 to -0.894), while FID increased by 67.5% (from 281.2 to 471.1) compared to Mist. Additionally, on the VGG-Face2 dataset with the prompt "a close-up photo of sks person, high details", HAA achieved a 43.8% reduction in FDSR (from 52.1% to 8.3%), a 7.8% reduction in Face Similarity (from 15.5% to 7.7%), and a 329.2% reduction in Image Reward (from 0.353 to -1.162), while FID increased by 34.4% (from 341.1 to 458.4) compared to CAAT. Clearly, HAA demonstrates a stronger capability for facial identity removal. Thanks to our unique design targeting Hierarchical Anti-Aesthetics, HAA enhances the ability to de-identify facial information, proving its effectiveness in protecting facial privacy and preventing the misuse of customized DMs.

TABLE III
EFFECTIVENESS STUDIES ACROSS VARYING NOISE BUDGETS.

eps	FDSR ↓	Face Similarity ↓	Image Reward ↓	FID ↑
0.00	1.000	0.498	0.599	112.3
0.01	0.781	0.493	0.556	117.2
0.05	0.250	0.220	-0.429	417.6
0.10	0.156	0.054	-0.999	462.2
0.15	**0.000**	**0.000**	**-1.364**	**497.0**

C. Parameter Tuning

In our method, there are two hyperparameters, λ and β defined in Eq. 15, where λ represents the weight of the global anti-aesthetic loss, and β represents the weight of

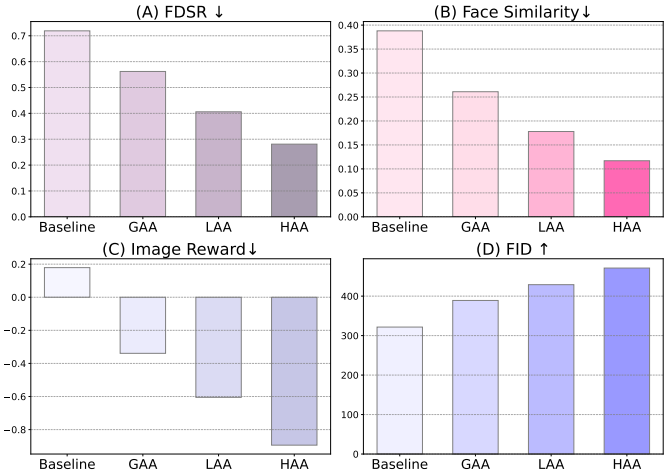

Fig. 5. Effectiveness Analysis of HAA Components.

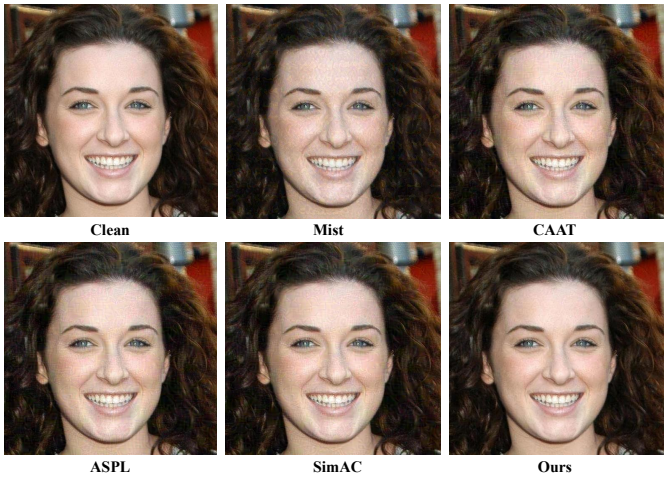

Fig. 6. Portrait image protected by different methods. The protective noise added by HAA on user images is subtle.

the local anti-aesthetic loss. We conducted parameter tuning experiments on the CelebA-HQ dataset using the SD-2.1 model and analyzed the impact of each parameter on the FID value. As shown in the Figure 4, changes in λ have a significant effect on the FID value. Initially, as λ increases, the FID rises, indicating that the introduction of global anti-aesthetics effectively degrades the overall image quality and enhances the adversarial attack capability. The FID reaches a peak when $\lambda = 0.2$ and then declines, so we set $\lambda = 0.2$ for subsequent experiments. β also has an important impact on the overall performance of the method. To achieve the best performance, similarly, we set $\beta = 0.2$.

D. Ablation Study

Effectiveness Analysis of HAA Components. Through systematic ablation studies, we thoroughly analyze the individual contributions of the Global Anti-Aesthetics (GAA) and Local Anti-Aesthetics (LAA) modules, as well as their synergistic effects. Figure 5 shows that, compared to the Baseline (FDSR = 0.719), the introduction of the GAA mechanism effectively reduces FDSR by 21.8% to 0.562 and Face Similarity

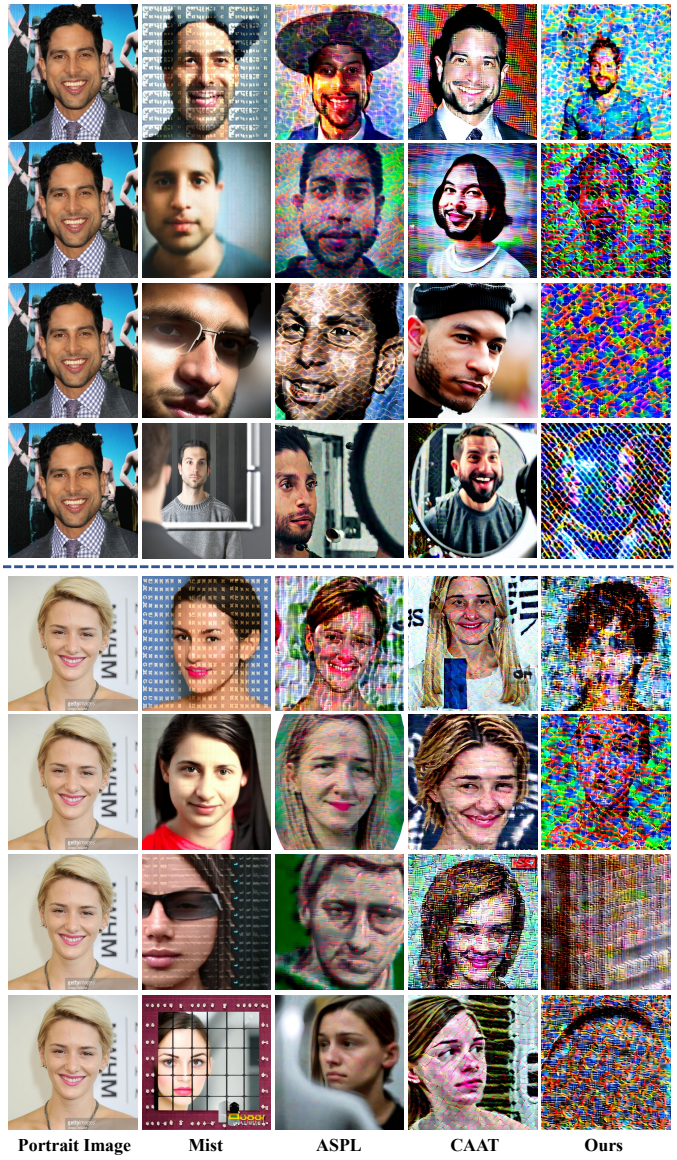

Fig. 7. Comparative visualization results on the VGGFace2 dataset. Two individuals and four prompts are used for experimental evaluation. Arranged from top to bottom, the prompts for each individual are as follows: "a photo of a sks person", "a DSLR portrait of a sks person", "a close-up photo of a sks person with high details", and "a photo of a sks person looking at the mirror".

by 32.7% to 0.261. Experiments demonstrate that GAA, by exploiting global aesthetic cues, suppresses the global aesthetic score of generated images, thereby enhancing the capacity to degrade image quality. Subsequently, by incorporating the local anti-facial aesthetics loss into the baseline method, we find that LAA outperforms GAA, with FDSR further reduced by 27.8% to 0.406 and Image Reward plummeting from -0.339 to -0.605. This indicates that localized, targeted anti-aesthetic loss significantly enhances the attack effect. Ultimately, the complete HAA method, which integrates both global and local anti-aesthetics, exhibits a synergistic effect: FDSR drops to 0.281 (a 60.9% reduction compared to the baseline), Face Similarity decreases by 69.8% to 0.117, Image Reward reaches -0.894, and the FID value increases by 46.5% to 471.1. This stepwise performance improvement clearly illustrates that the

TABLE IV
ASSESSMENT ACROSS DIFFERENT DMS VERSIONS.

SD-V1.4				
attack	FDSR↓	Face Similarity↓	Image Reward↓	FID↑
Clean	0.938	0.439	0.440	148.4
Mist	0.906	0.332	-0.027	237.8
CAAT	0.125	0.035	-1.083	508.8
ASPL	0.375	0.076	-0.728	458.4
SimAC	0.186	0.067	-1.079	508.1
HAA	**0.062**	**0.030**	**-1.577**	**540.4**
SD-V1.5				
attack	FDSR↓	Face Similarity↓	Image Reward↓	FID↑
Clean	0.969	0.454	0.577	140.4
Mist	1.000	0.383	-0.165	225.9
CAAT	0.312	0.036	-1.335	466.5
ASPL	0.250	0.059	-0.904	479.4
SimAC	0.219	0.149	-1.230	452.8
HAA	**0.000**	**0.003**	**-1.563**	**523.7**

TABLE V
HAA AGAINST DIVERSE IMAGE PERTURBATION METHODS.

Method	FDSR ↓	Face Similarity ↓	Image Reward ↓	FID ↑
clean	1.000	0.498	0.599	112.3
HAA	**0.281**	**0.117**	**-0.894**	**471.1**
gas k=3	0.644	0.302	0.315	215.1
gas k=5	0.875	0.326	0.377	215.6
gas k=7	0.906	0.349	0.410	209.1
jep q=30	0.938	0.269	-0.537	257.2
jep q=50	0.869	0.262	-0.488	263.2
jep q=70	0.813	0.254	-0.373	267.0

global mechanism established by GAA and the localized precision attacks of LAA complement each other. Through multi-level, multi-scale synergistic effects, HAA ultimately achieves the maximum destruction of the malicious fine-tuners' reconstruction capabilities while maintaining the stealth of the attack. , providing a solution for protecting user privacy.

Effectiveness studies across varying noise budgets. We examine the impact of different perturbation budgets on the generation quality of customized models, When applying HAA. Table III shows the results with perturbation budgets (eps) set to 0.0, 0.01, 0.05, 0.1, and 0.15. Experiments indicate that larger budgets lead to more pronounced degradation in image quality. However, using excessively large perturbation budgets is unreasonable, as it can severely affect the use of the protected images. The noise added by HAA is subtle, it can still effectively fortify users' portrait rights.

E. More Results

Visualization Results. As shown in Figure 6, the protective noise added by GAA is minimal and barely affects the aesthetic quality of the user's image. Figure 7 illustrates the visual attack effects of different methods on T2I models. It can be observed that HAA effectively enhances the ability to remove identity information, protecting users' facial privacy and copyright.

Black-Box Performance on different DMs versions. To simulate real-world scenarios where target T2I models may not be consistent with the surrogate models, we test different versions of diffusion models to examine the stability of HAA in black-box settings. As shown in Table IV, HAA demonstrates stable performance on both SD-v1.4 and SD-v1.5, indicating its excellent generalization ability. This confirms that HAA can effectively counter attacks under various conditions while effectively disrupting identity information in images.

Robustness of HAA. To verify whether HAA can cope with distortions, compression damage, blurring, and other situations in real-world application scenarios, we conducted robustness tests on HAA using multiple image perturbation methods. We utilized Gaussian blur and JPEG compression with varying intensities, denoted by kernel size k and quality q, to remove adversarial protection. Table V shows that our method still successfully attacks T2I models under various image perturbations, proving its effectiveness and robustness. The supplementary materials demonstrate the effectiveness of HAA across more fine-tuning scenarios.

V. CONCLUSION

Existing anti-customization methods often overlook key aesthetic clues, limiting their ability to remove identities. To address this issue, we propose a Hierarchical Anti-Aesthetic (HAA) framework, which includes both Global Anti-Aesthetics and Local Anti-Aesthetics branches. These branches work together to fully mine aesthetic clues from global to local, forcing customized DMs to undergo anti-human preference aesthetic alignment, thereby effectively reducing their ability to reconstruct facial details. Our experiments demonstrate that HAA outperforms existing methods and provides a powerful tool for protecting facial privacy and copyright.

REFERENCES

[1] S. Gu, D. Chen, J. Bao, F. Wen, B. Zhang, D. Chen, L. Yuan, and B. Guo, "Vector quantized diffusion model for text-to-image synthesis," in *Proceedings of the IEEE/CVF conference on computer vision and pattern recognition*, 2022, pp. 10 696–10 706.

[2] R. Rombach, A. Blattmann, D. Lorenz, P. Esser, and B. Ommer, "High-resolution image synthesis with latent diffusion models," in *Proceedings of the IEEE/CVF conference on computer vision and pattern recognition*, 2022, pp. 10 684–10 695.

[3] A. Ramesh, P. Dhariwal, A. Nichol, C. Chu, and M. Chen, "Hierarchical text-conditional image generation with clip latents," *arXiv preprint arXiv:2204.06125*, vol. 1, no. 2, p. 3, 2022.

[4] J. Ho, A. Jain, and P. Abbeel, "Denoising diffusion probabilistic models," *Advances in neural information processing systems*, vol. 33, pp. 6840–6851, 2020.

[5] J. Song, C. Meng, and S. Ermon, "Denoising diffusion implicit models," *arXiv preprint arXiv:2010.02502*, 2020.

[6] O. Bar-Tal, D. Ofri-Amar, R. Fridman, Y. Kasten, and T. Dekel, "Text2live: Text-driven layered image and video editing," in *European conference on computer vision*. Springer, 2022, pp. 707–723.

[7] G. Kim, T. Kwon, and J. C. Ye, "Diffusionclip: Text-guided diffusion models for robust image manipulation," in *Proceedings of the IEEE/CVF Conference on Computer Vision and Pattern Recognition*, 2022, pp. 2426–2435.

[8] R. Gal, Y. Alaluf, Y. Atzmon, O. Patashnik, A. H. Bermano, G. Chechik, and D. Cohen-Or, "An image is worth one word: Personalizing text-to-image generation using textual inversion," *arXiv preprint arXiv:2208.01618*, 2022.

[9] N. Ruiz, Y. Li, V. Jampani, Y. Pritch, M. Rubinstein, and K. Aberman, "Dreambooth: Fine tuning text-to-image diffusion models for subject-driven generation," in *Proceedings of the IEEE/CVF conference on computer vision and pattern recognition*, 2023, pp. 22 500–22 510.

[10] N. Kumari, B. Zhang, R. Zhang, E. Shechtman, and J.-Y. Zhu, "Multi-concept customization of text-to-image diffusion," in *Proceedings of the IEEE/CVF Conference on Computer Vision and Pattern Recognition*, 2023, pp. 1931–1941.

[11] L. Han, Y. Li, H. Zhang, P. Milanfar, D. Metaxas, and F. Yang, "Svdiff: Compact parameter space for diffusion fine-tuning," in *Proceedings of the IEEE/CVF International Conference on Computer Vision*, 2023, pp. 7323–7334.

[12] J. Vice, N. Akhtar, R. Hartley, and A. Mian, "Bagm: A backdoor attack for manipulating text-to-image generative models," *IEEE Transactions on Information Forensics and Security*, 2024.

[13] Y. Huang, F. Juefei-Xu, Q. Guo, J. Zhang, Y. Wu, M. Hu, T. Li, G. Pu, and Y. Liu, "Personalization as a shortcut for few-shot backdoor attack against text-to-image diffusion models," in *Proceedings of the AAAI Conference on Artificial Intelligence*, vol. 38, no. 19, 2024, pp. 21 169–21 178.

[14] J. Frank, T. Eisenhofer, L. Schönherr, A. Fischer, D. Kolossa, and T. Holz, "Leveraging frequency analysis for deep fake image recognition," in *International conference on machine learning*. PMLR, 2020, pp. 3247–3258.

[15] B. Zheng, C. Liang, X. Wu, and Y. Liu, "Understanding and improving adversarial attacks on latent diffusion model," *arXiv preprint arXiv:2310.04687*, 2023.

[16] T. Van Le, H. Phung, T. H. Nguyen, Q. Dao, N. N. Tran, and A. Tran, "Anti-dreambooth: Protecting users from personalized text-to-image synthesis," in *Proceedings of the IEEE/CVF International Conference on Computer Vision*, 2023, pp. 2116–2127.

[17] J. Xu, Y. Lu, Y. Li, S. Lu, D. Wang, and X. Wei, "Perturbing attention gives you more bang for the buck: Subtle imaging perturbations that efficiently fool customized diffusion models," in *Proceedings of the IEEE/CVF Conference on Computer Vision and Pattern Recognition*, 2024, pp. 24 534–24 543.

[18] P. P. Tinio, H. Leder, and M. Strasser, "Image quality and the aesthetic judgment of photographs: Contrast, sharpness, and grain teased apart and put together." *Psychology of Aesthetics, Creativity, and the Arts*, vol. 5, no. 2, p. 165, 2011.

[19] S. E. Palmer, K. B. Schloss, and J. Sammartino, "Visual aesthetics and human preference," *Annual review of psychology*, vol. 64, no. 1, pp. 77–107, 2013.

[20] V. Gallego, "Personalizing text-to-image generation via aesthetic gradients," *arXiv preprint arXiv:2209.12330*, 2022.

[21] S. Wu, F. Ding, M. Huang, W. Liu, and Q. He, "Vmix: Improving text-to-image diffusion model with cross-attention mixing control," *arXiv preprint arXiv:2412.20800*, 2024.

[22] J. Ho, C. Saharia, W. Chan, D. J. Fleet, M. Norouzi, and T. Salimans, "Cascaded diffusion models for high fidelity image generation," *Journal of Machine Learning Research*, vol. 23, no. 47, pp. 1–33, 2022.

[23] A. Lugmayr, M. Danelljan, A. Romero, F. Yu, R. Timofte, and L. Van Gool, "Repaint: Inpainting using denoising diffusion probabilistic models," in *Proceedings of the IEEE/CVF Conference on Computer Vision and Pattern Recognition*, 2022, pp. 11 461–11 471.

[24] D. Podell, Z. English, K. Lacey, A. Blattmann, T. Dockhorn, J. Müller, J. Penna, and R. Rombach, "Sdxl: Improving latent diffusion models for high-resolution image synthesis," *arXiv preprint arXiv:2307.01952*, 2023.

[25] A. Radford, J. W. Kim, C. Hallacy, A. Ramesh, G. Goh, S. Agarwal, G. Sastry, A. Askell, P. Mishkin, J. Clark *et al.*, "Learning transferable visual models from natural language supervision," in *International conference on machine learning*. PMLR, 2021, pp. 8748–8763.

[26] C. Liang, X. Wu, Y. Hua, J. Zhang, Y. Xue, T. Song, Z. Xue, R. Ma, and H. Guan, "Adversarial example does good: Preventing painting imitation from diffusion models via adversarial examples," *arXiv preprint arXiv:2302.04578*, 2023.

[27] F. Wang, Z. Tan, T. Wei, Y. Wu, and Q. Huang, "Simac: a simple anti-customization method for protecting face privacy against text-to-image synthesis of diffusion models," in *Proceedings of the IEEE/CVF Conference on Computer Vision and Pattern Recognition*, 2024, pp. 12 047–12 056.

[28] J. Xu, X. Liu, Y. Wu, Y. Tong, Q. Li, M. Ding, J. Tang, and Y. Dong, "Imagereward: Learning and evaluating human preferences for text-to-image generation," *Advances in Neural Information Processing Systems*, vol. 36, 2024.

[29] H. Zhu, W. Wu, W. Zhu, L. Jiang, S. Tang, L. Zhang, Z. Liu, and C. C. Loy, "Celebv-hq: A large-scale video facial attributes dataset," in *European conference on computer vision*. Springer, 2022, pp. 650–667.

[30] Q. Cao, L. Shen, W. Xie, O. M. Parkhi, and A. Zisserman, "Vggface2: A dataset for recognising faces across pose and age," in *2018 13th IEEE international conference on automatic face & gesture recognition (FG 2018)*. IEEE, 2018, pp. 67–74.

[31] R. Rombach, A. Blattmann, D. Lorenz, P. Esser, and B. Ommer, "High-resolution image synthesis with latent diffusion models," 2021.

[32] ——, "High-resolution image synthesis with latent diffusion models," in *Proceedings of the IEEE/CVF Conference on Computer Vision and Pattern Recognition (CVPR)*, June 2022, pp. 10 684–10 695.

[33] S. Yang, P. Luo, C.-C. Loy, and X. Tang, "From facial parts responses to face detection: A deep learning approach," in *Proceedings of the IEEE international conference on computer vision*, 2015, pp. 3676–3684.

[34] J. N. Bailenson, S. Iyengar, N. Yee, and N. A. Collins, "Facial similarity between voters and candidates causes influence," *Public opinion quarterly*, vol. 72, no. 5, pp. 935–961, 2008.

[35] M. Heusel, H. Ramsauer, T. Unterthiner, B. Nessler, and S. Hochreiter, "Gans trained by a two time-scale update rule converge to a local nash equilibrium," *Advances in neural information processing systems*, vol. 30, 2017.